Electronic Supplementary Material (ESI) for Biomaterials Science.
This journal is © The Royal Society of Chemistry 2022

Supporting Information

Modulation of Hypoxia and Redox in Solid Tumor Microenvironment with a Catalytic Nanoplatform to Enhance Combinational Chemodynamic/Sonodynamic Therapy

Yeping Liu, Likai Wang, Fengyuan Wei, Ya Tian, Juan Mou*, Shiping Yang, Huixia Wu*

The Education Ministry Key Lab of Resource Chemistry, Joint International Research Laboratory of Resource Chemistry, Ministry of Education, Shanghai Key Laboratory of Rare Earth Functional Materials, Shanghai Municipal Education Committee Key Laboratory of Molecular Imaging Probes and Sensors, and Shanghai Frontiers Science Center of Biomimetic Catalysis, College of Chemistry and Materials Science, Shanghai Normal University, Shanghai 200234, China

E-mail: moujuan@shnu.edu.cn, wuhuixia@shnu.edu.cn

Materials

Melamine, protoporphyrin IX (PpIX), 1,3-diphenylisobenzofuran (DPBF), 9,10-anthracenediyl-bis(methylene) dimalonic acid (ABDA), 3,3',5,5'-tetramethylbenzidine (TMB), amiloride hydrochloride ($C_6H_8ClN_7O{\cdot}HCl$), chlorpromazine hydrochloride ($C_{17}H_{20}Cl_2N_2S$), and genistein ($C_{15}H_{10}O_5$) were purchased from Shanghai Macklin Biochemical Technology Co., Ltd. Potassium permanganate ($KMnO_4$) was provided by Shanghai Titan Technology Co., Ltd. Manganese (II) acetate tetrahydrate ($Mn(CH_3COO)_2{\cdot}4H_2O$) was acquired from Sinopharm Chemical Reagent Co., Ltd. Triethylamine (TEA, $C_6H_{15}N$) was supplied by Shanghai Richjoint Chemical Co., Ltd.

Bovine albumin (BSA) was purchased from Amresco (Solon, OH, USA). Glutathione (GSH) was obtained from Acros. 5,5′-Dithiobis(2-nitrobenzoic acid) was bought from Adamas. 3-(4,5-Dimethylthiazol-2-yl)-2,5-diphenyltetrazolium bromide (MTT) was provided by Meryer Chemical Technology Co., Ltd. 2',7'-Dichlorodihydrofluorescein diacetate (DCFH-DA) was obtained from Beyotime Biotechnology Co., Ltd. Calcein-AM/PI double stain kit was purchased from Yeasen Biotechnology Co., Ltd. All reagents were used as received without further purification. Deionized water with a resistivity higher than 18 MΩ cm was used in all relevant experiments.

Characterizations

Transmission electron microscopy (TEM) images were acquired on a JEOL JEM-2199 high-resolution transmission electron microscope. Elemental mappings were measured using an FEI Talos F200S/F200X transmission electron microscope. Atomic force microscopy (AFM) measurement was performed with a NT-MDT NTEGRA spectra system. The zeta potentials were measured with a Malvern Zetasizer ZEN3690 analyzer. Ultraviolet-visible (UV-vis) absorption spectra were recorded on a BeckMan coulter DU 730 spectrophotometer. Fourier transform infrared (FT-IR) spectra were collected on a Nicolet Avatar 370 spectrophotometer. The fluorescence spectra were achieved on a Cary Eclipse fluorescence spectrophotometer. X-ray diffraction (XRD) analysis was carried out using a Rigaku DMAX 2000 diffractometer with Cu-Kα radiation (λ = 0.15405 nm). X-ray photoelectron spectroscopy (XPS) was conducted using an AXIS-165 X-ray spectrometer (Kratos).

Supplementary figures

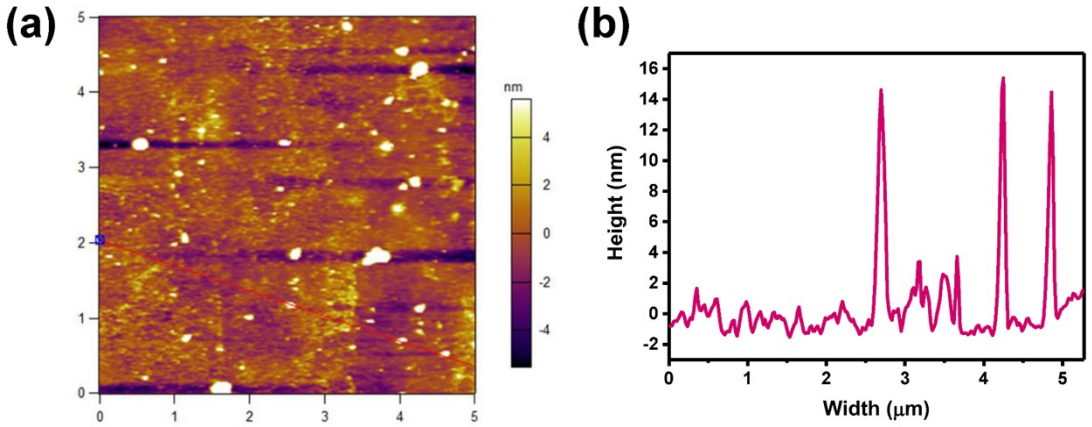

Fig. S1 AFM image (a) and the height profile (b) of OCN nanosheets.

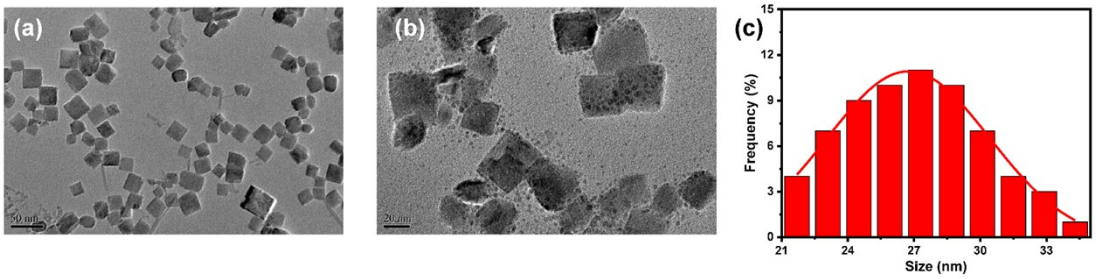

Fig. S2 TEM images (a-b) and size distribution of pure Mn_3O_4 derived without the addition of OCN.

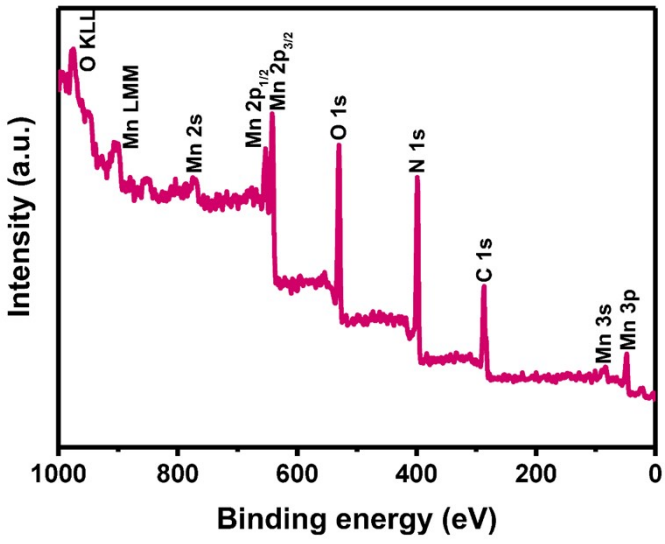

Fig. S3 The XPS survey spectrum of Mn_3O_4/OCN.

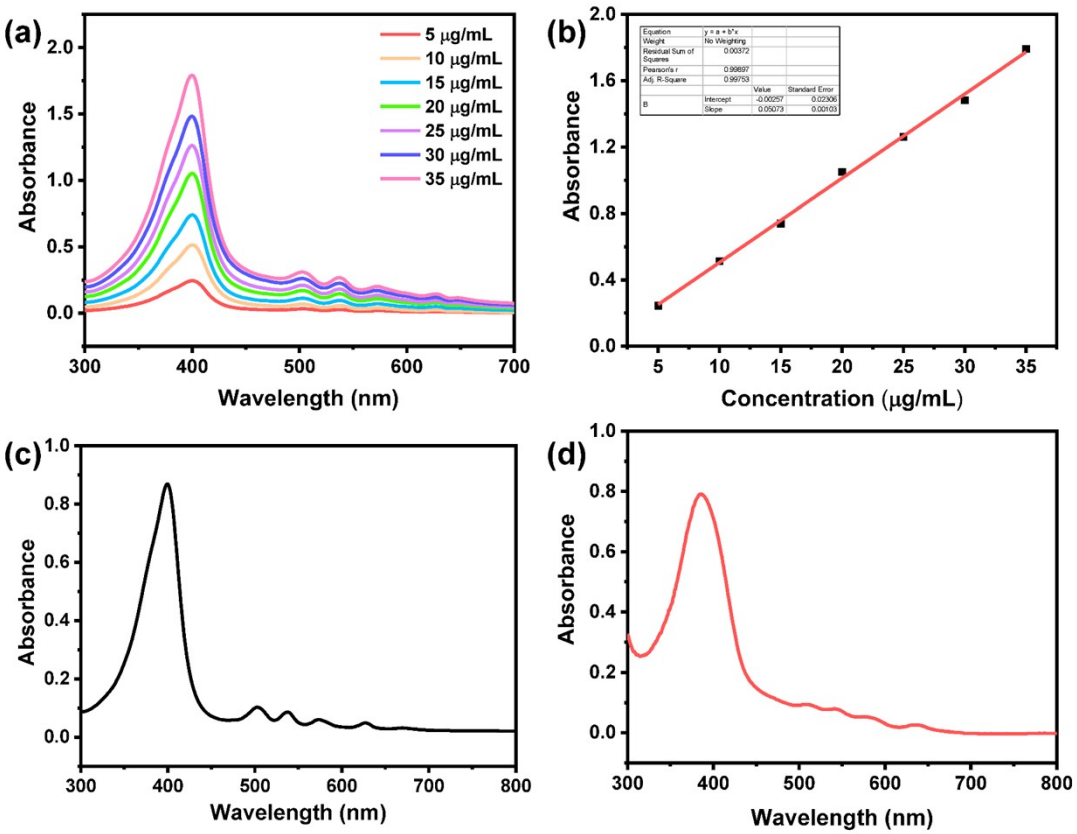

Fig. S4 (a) UV-Vis absorption spectra of PpIX aqueous solution at different concentrations and corresponding standard curve of PpIX aqueous solution. UV-Vis absorption spectra of the supernatant of Mn_3O_4-PpIX (c) and Mn_3O_4/OCN- PpIX (d).

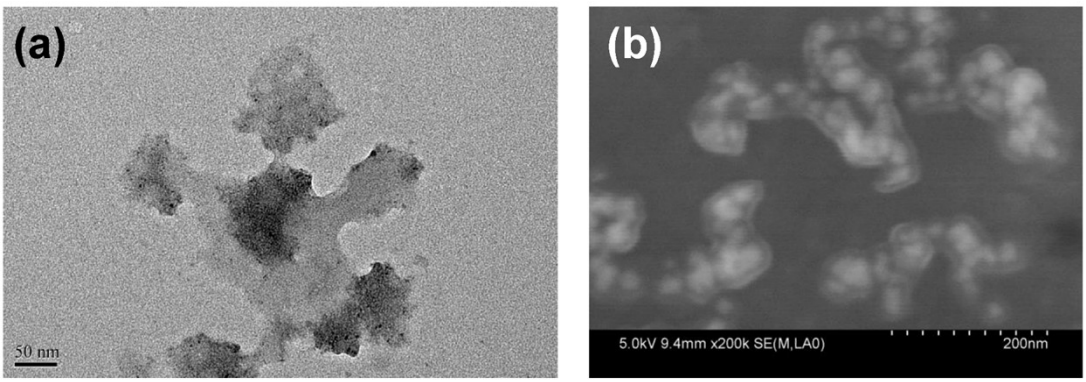

Fig. S5 TEM (a) and SEM (b) images of Mn_3O_4/OCN-PpIX@BSA.

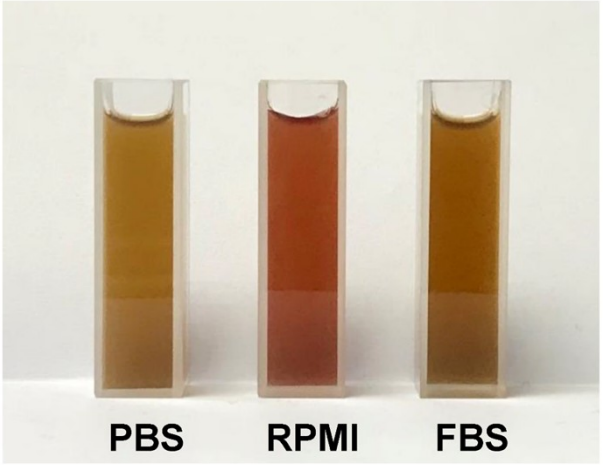

Fig. S6 The photographs of Mn_3O_4/OCN-PpIX@BSA dispersed in PBS, RPMI-1640, and FBS solution, respectively.

Fig. S7 Photograph of the mixture of OCN (400 μg/mL) and H_2O_2 (10 mM), showing no apparent bubble generation.

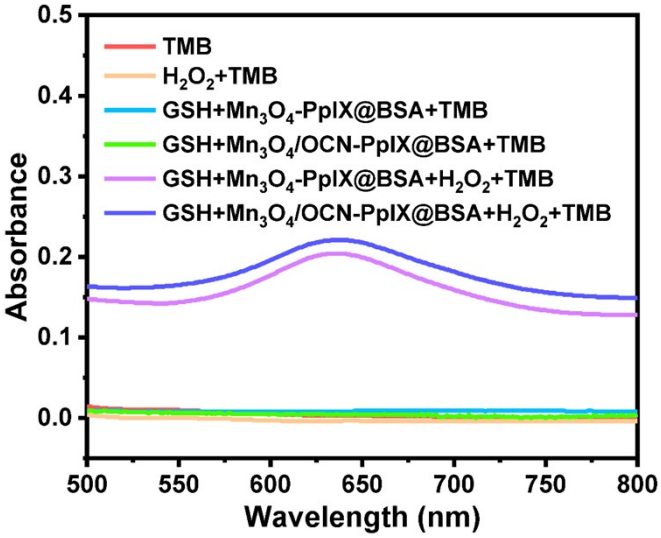

Fig. S8 Absorption spectra of oxidized TMB in various solution systems.

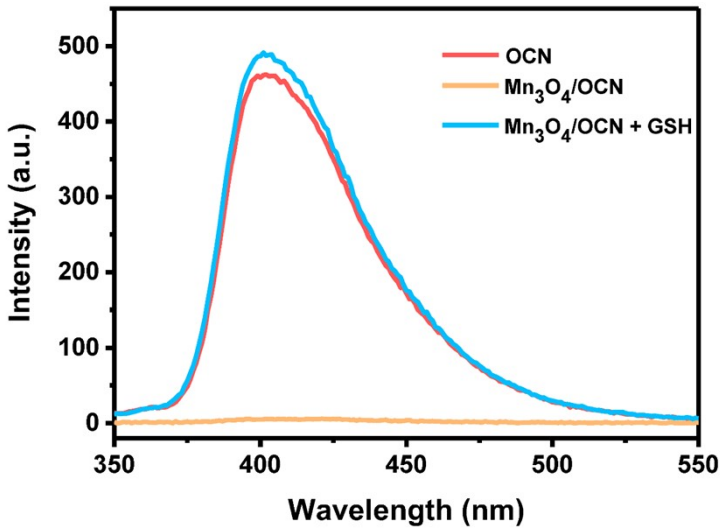

Fig. S9 Fluorescence spectra of OCN, Mn_3O_4/OCN, and Mn_3O_4/OCN treated with GSH.

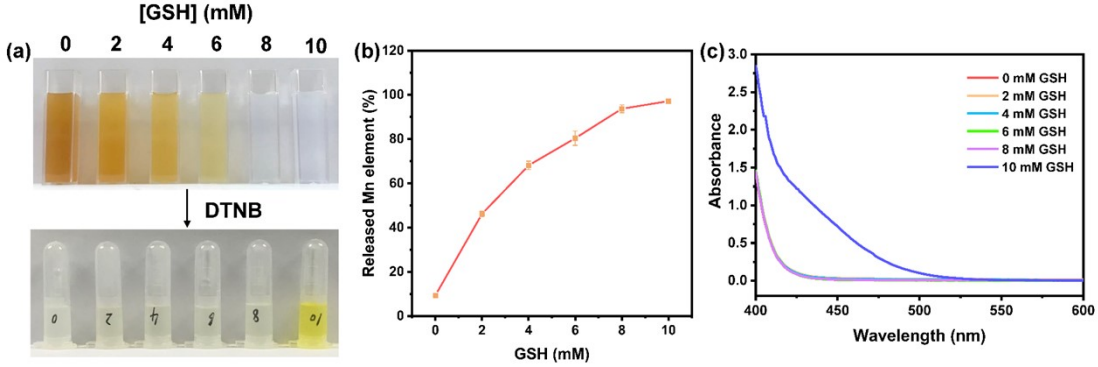

Fig. S10 (a) Photographs showing the degradation behavior of Mn_3O_4/OCN (OCN: white color) with a concentration of 400 μg/mL in different concentrations of GSH solutions (upper row) and the detection of remaining GSH in the supernatant (lower row). (b) The release percentage of Mn in the supernatant determined by ICP-AES. (c) The corresponding absorption spectra of the solutions showed in the lower row of (a).

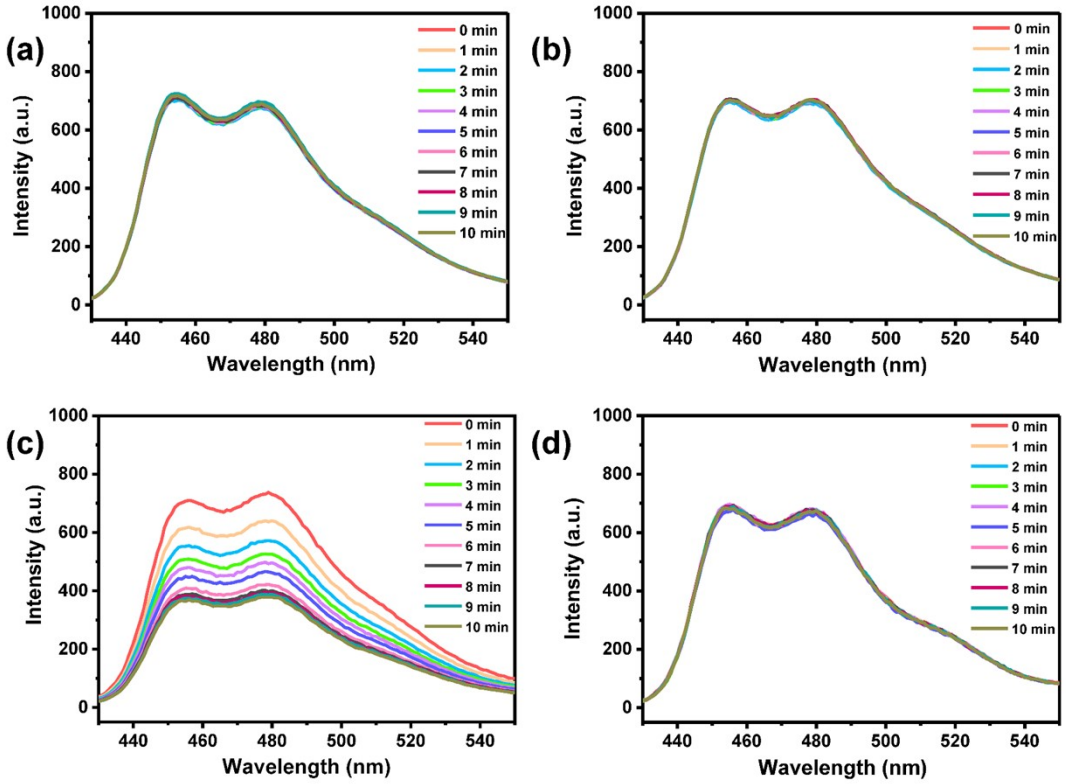

Fig. S11 Fluorescence spectra of DPBF in different groups after US irradiation: (a) DPBF only (control group); (b) DPBF + Mn_3O_4/OCN@BSA; (c) DPBF + Mn_3O_4/OCN-PpIX@BSA; (d) DPBF + Mn_3O_4/OCN-PpIX@BSA + NaN_3 (Inhibition group).

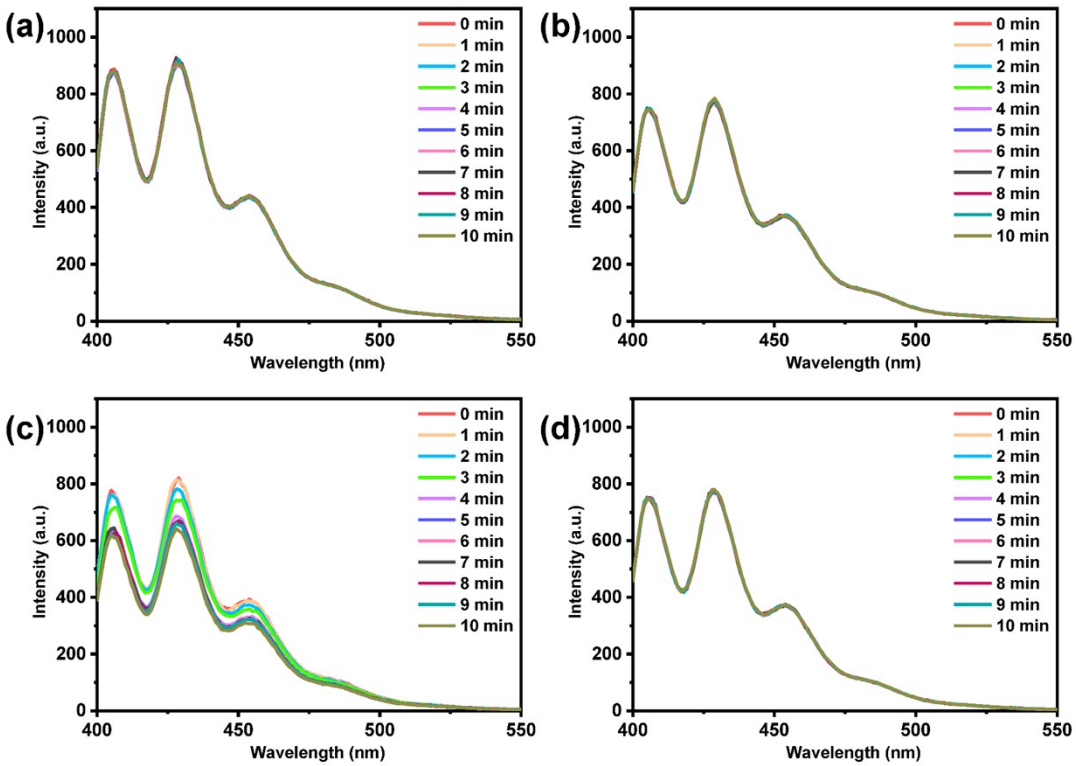

Fig. S12 Fluorescence spectra of ABDA in different groups after US irradiation: (a) ABDA only (control group); (b) ABDA + Mn_3O_4/OCN@BSA; (c) ABDA + Mn_3O_4/OCN-PpIX@BSA; (d) ABDA + Mn_3O_4/OCN-PpIX@BSA + NaN_3 (Inhibition group).

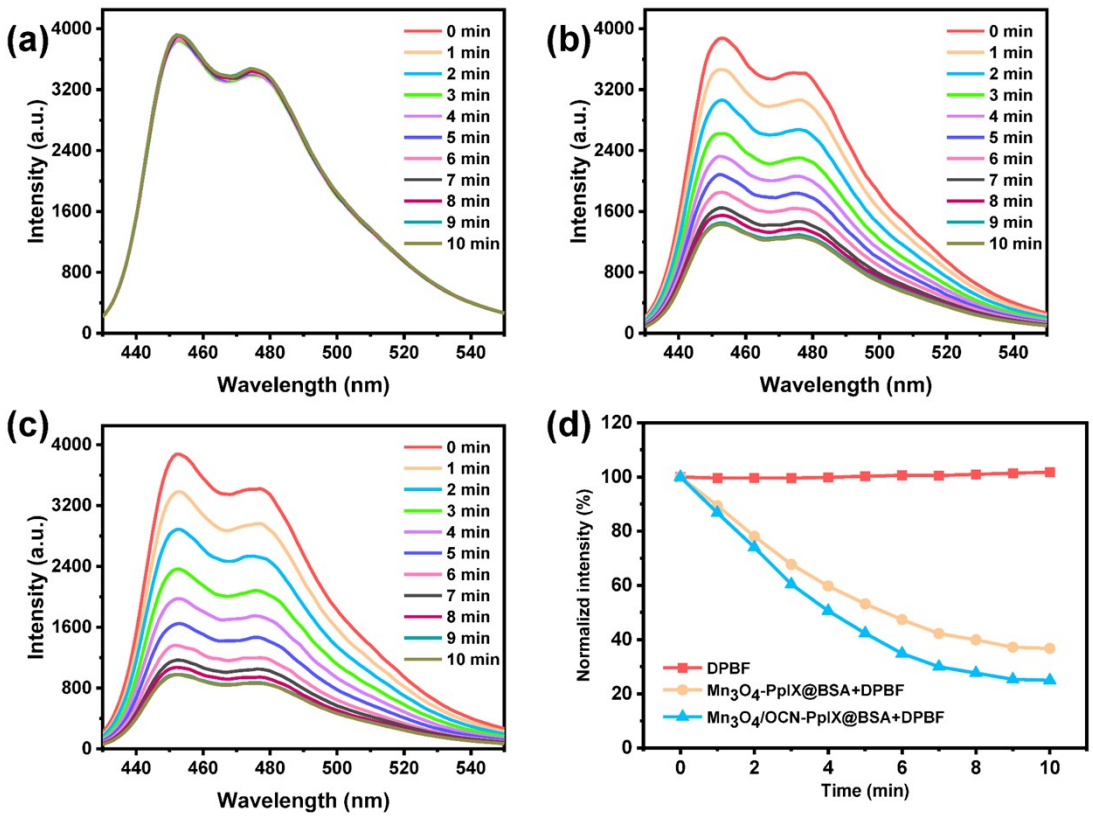

Fig. S13 Fluorescence spectra of DPBF in different groups after US irradiation: (a) DPBF only (control group); (b) DPBF + Mn_3O_4-PpIX@BSA; (c) DPBF + Mn_3O_4/OCN-PpIX@BSA. (d) Changes in the fluorescence intensity of DPBF (λ_{em}=456 nm) with US irradiation time (power density = 1 W/cm^2, frequency = 1 MHz, duty cycle = 50%, and pulse frequency = 100 Hz) in different groups. Mn concentration: 50 μM.

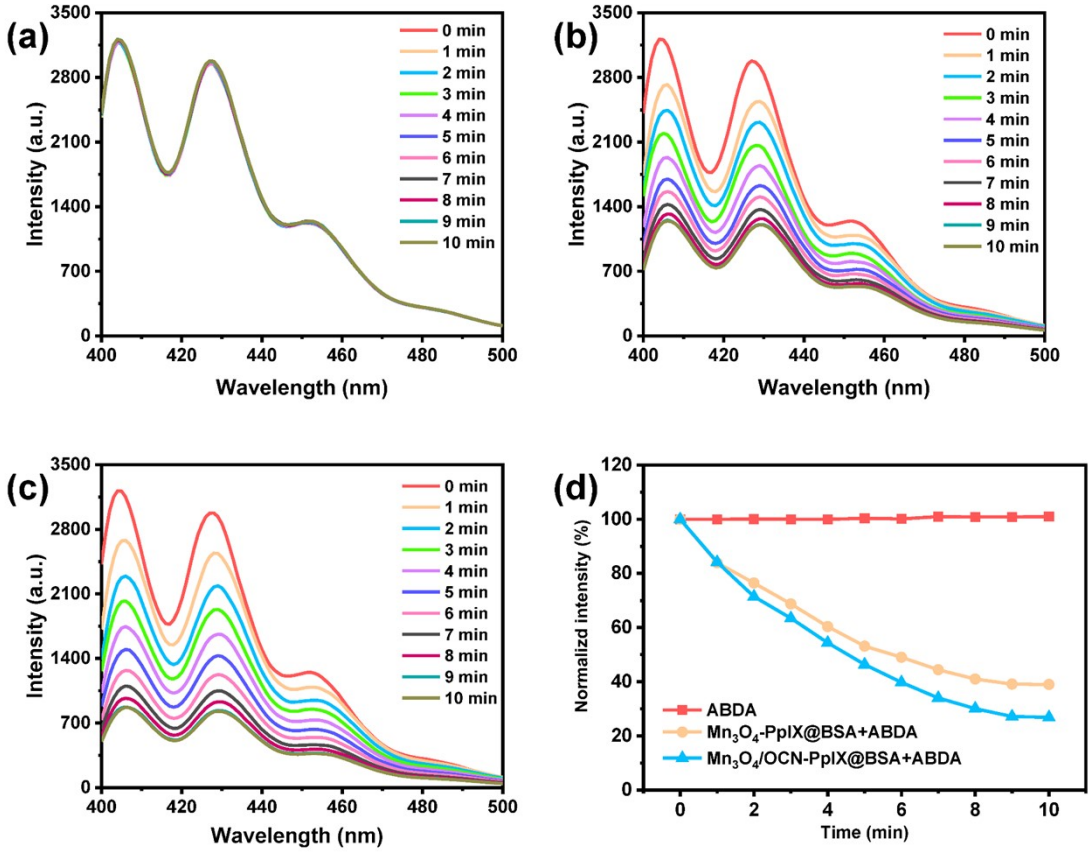

Fig. S14 Fluorescence spectra of ABDA in different groups after US irradiation: (a) ABDA only (control group); (b) ABDA + Mn_3O_4-PpIX@BSA; (c) ABDA + Mn_3O_4/OCN-PpIX@BSA. (d) Changes in fluorescence intensity of ABDA (λ_{em}=427 nm) with US irradiation time (power density = 1 W/cm^2, frequency = 1 MHz, duty cycle = 50%, and pulse frequency = 100 Hz) in different groups. Mn concentration: 50 μM.

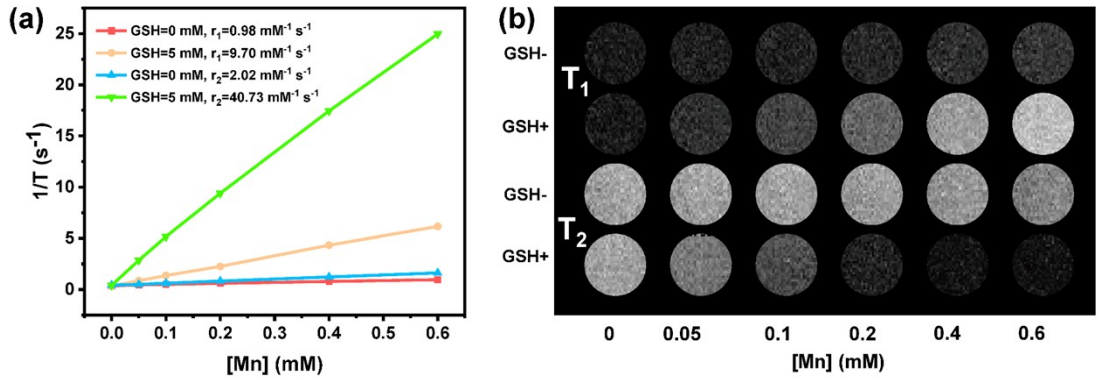

Fig. S15 (a) Plots of 1/T as a function of Mn concentration for Mn_3O_4-PpIX@BSA and Mn_3O_4-PpIX@BSA + GSH (5 mM). (b) Corresponding T_1- and T_2-weighted MRI images for Mn_3O_4-PpIX@BSA treated with GSH (5 mM) or not.

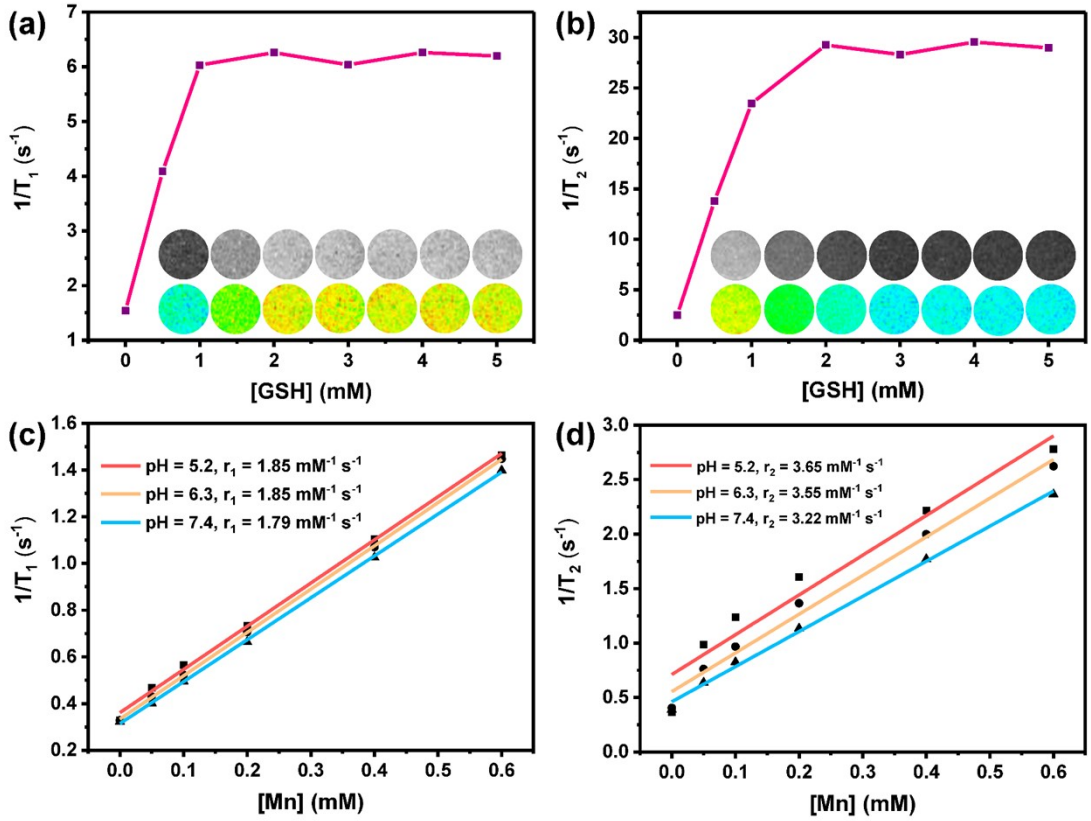

Fig. S16 T_1 (a) and T_2 (b) relaxation rate ($1/T_1$, $1/T_2$) together with corresponding MRI images for Mn_3O_4/OCN-PpIX@BSA in different concentrations of GSH solution ([Mn] = 0.6 mM). $1/T_1$ (c) and $1/T_2$ (d) values of Mn_3O_4/OCN-PpIX@BSA in PBS solutions with different pH as a function of Mn^{2+} concentration.

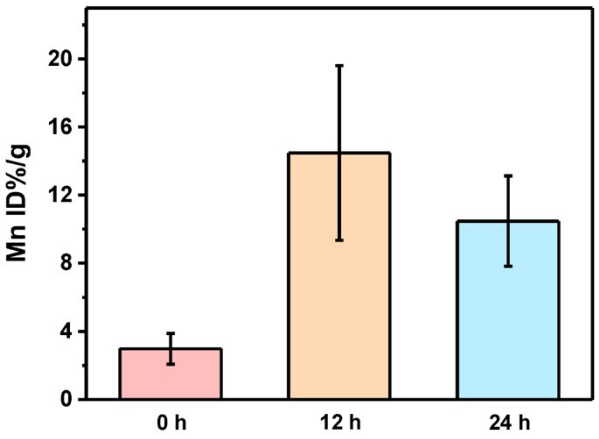

Fig. S17 Mn element concentration in tumors measured by ICP-AES before (0 h) and after (12 and 24 h post-injection) intravenous injection of Mn_3O_4/OCN-PpIX@BSA (3 mice per group).